Asian Journal of Urology (2019) 6, 256–263

Available online at www.sciencedirect.com

ScienceDirect

journal homepage: www.elsevier.com/locate/ajur

Original Article

Multiparametric MRI reporting using Prostate Imaging Reporting and Data System version 2.0 (PI-RADSv2) retains clinical efficacy in a predominantly post-biopsy patient population

Edwin Jonathan Aslim [a], Yan Mee Law [b], Puay Hoon Tan [c], John Carson Allen Jr [d], Lionel Tim-Ee Cheng [b], Viswanath Anand Chidambaram [b], Li Yan Khor [e], Benjamin Yongcheng Tan [e], Ernest Wencong Eu [a], Christopher Wai Sam Cheng [a], John Shyi Peng Yuen [a], Henry Sun Sien Ho [a], Lui Shiong Lee [a,*]

[a] *Department of Urology, Singapore General Hospital, Singapore*
[b] *Department of Diagnostic Radiology, Singapore General Hospital, Singapore*
[c] *Division of Pathology, Singapore General Hospital, Singapore*
[d] *Centre of Quantitative Medicine, DUKE-NUS Medical School, Singapore*
[e] *Department of Anatomical Pathology, Singapore General Hospital, Singapore*

Received 7 March 2017; received in revised form 12 April 2017; accepted 14 November 2017
Available online 1 June 2018

KEYWORDS
Gleason score;
Histopathology;
Magnetic resonance imaging;
Prostatectomy;
Prostatic cancer

Abstract *Objective:* To evaluate the efficacy of multiparametric magnetic resonance imaging (mp-MRI) using Prostate Imaging Reporting and Data System version 2.0 (PI-RADSv2) definitions in detecting organ-confined prostate cancer.
Methods: All patients who underwent radical prostatectomy between January 1, 2014 and December 30, 2014 were identified. All underwent mp-MRI within 180 days before surgery. Those with prior pelvic irradiation or androgen deprivation therapy were excluded. Fully embedded, whole-mount histopathology was centrally reviewed and correlated with imaging for tumour location, Gleason score (GS) and stage.
Results: There were 39 patients included, of which 35 (90%) had mp-MRI done post-biopsy. A total of 93 cancer foci were identified on whole-mount pathology, of which mp-MRI detected

* Corresponding author.
E-mail address: lee.lui.shiong@singhealth.com.sg (L.S. Lee).
Peer review under responsibility of Second Military Medical University.

https://doi.org/10.1016/j.ajur.2018.05.008

63 (68%). Of those detected by mp-MRI, 14 were PI-RADS 3 ($n = 6$ for GS 6, $n = 8$ for GS 7, no GS ≥ 8) and 49 were PI-RADS 4–5 ($n = 7$ for GS 6, $n = 33$ for GS 7, and $n = 9$ for GS ≥ 8). There were 30 (32%) cancer foci missed by mp-MRI ($n = 15$ for GS 6, $n = 13$ for GS 7 and $n = 2$ for GS ≥ 8). A lesion classified as PI-RADS 4–5 predicted a higher grade cancer on pathology as compared to PI-RADS 3 (for GS 7 lesions, odds ratio [OR] = 3.53, 95% CI: 0.93–13.45, $p = 0.064$). The mp-MRI size detection limit was 20 mm^2 and 100 mm^2 for 50% and 75% probability of cancer, respectively. In associating with radiological and pathologic stage, the weighted Kappa value was 0.69 ($p < 0.0001$). The sensitivity and positive predictive values for this study were 68% (95% CI: 57%–77%) and 78% (95% CI: 67%–86%), respectively.
Conclusion: In this predominantly post-biopsy cohort, mp-MRI using PI-RADSv2 reporting has a reasonably high diagnostic accuracy in detecting clinically significant prostate cancer.

1. Introduction

Recent advances in multiparametric magnetic resonance imaging (mp-MRI) that have expanded its role in the diagnosis of organ confined prostate were focused mainly on a lack of standardized reporting methods, which led to widely variable diagnostic performance (different Likert scales) [1,2]. In 2012, the European Society of Urogenital Radiology (ESUR) introduced a set of consensus guidelines to standardize prostate magnetic resonance imaging (MRI) interpretations, referred to as Prostate Image Reporting and Data System (PI-RADS) [3]. However, due to a lack of integration of the PI-RADS scores from different imaging sequences, there was heterogeneity in the suspicion threshold across studies [4]. Prostate Image Reporting and Data System Version 2.0 (PIRADSv2) was published in April 2015, and provided standardized recommendations on the technical specifications of image acquisition, reporting methods, and integration of mp-MRI scores according to prostate zonal anatomy (Table 1) [5]. However, there are limited reports in literature on the efficacy of PI-RADSv2, with some initial data suggesting it had limited efficacy [6].

The purpose of this study was to evaluate the diagnostic performance of mp-MRI, using PI-RADSv2 recommendations in real-life clinical practice. The following outcomes were analysed:

(1) Correlation between mp-MRI PI-RADS score and pathological Gleason score (GS);
(2) Size detection limit of mp-MRI for malignant lesions;
(3) Location of tumours not detected by mp-MRI;
(4) Impact of the time interval between needle biopsy of the prostate and mp-MRI accuracy in detecting tumours.

Table 1 Prostate Imaging Reporting and Data System Version 2 (PI-RADSv2) grading method.

Peripheral zone				Transition zone			
DWI	T2W	DCE	PI-RADS score	T2W	DWI	DCE	PI-RADS score
1	Any	Any	1	1	Any	Any	1
2	Any	Any	2	2	Any	Any	2
3	Any	−	3	3	≤4	Any	3
		+	4		5	Any	4
4	Any	Any	4	4	Any	Any	4
5	Any	Any	5	5	Any	Any	5

Mp-MRI scores from all sequences were integrated into a single PI-RADS score, based on zonal anatomy of the lesion. DCE, dynamic contrast enhanced imaging; DWI, diffusion weighted imaging; T2W, T2 weighted imaging. Any denotes a score of 1–5. "+" denotes the presence of early enhancement on DCE, while "−" denotes the absence of it [5].

2. Materials and methods

2.1. Patient cohort

Following institutional review board approval (No. CIRB 2009/743/D), all patients who underwent radical prostatectomy as primary treatment for biopsy proven primary adenocarcinoma of the prostate gland, between January 1, 2014 and December 30, 2014, were identified. A prospectively maintained clinical registry provided data on the clinical characteristics of these patients. Only those who had mp-MRI within 180 days of surgery were included. Those who had prior pelvic irradiation or neo-adjuvant androgen deprivation therapy were excluded from this study. From this, a total of 39 patients with a median age of 64 years (range 45–74 years) were identified.

All relevant mp-MRI images and fully embedded whole mount histopathology were centrally reviewed by one dedicated uro-radiologist and one uro-pathologist respectively. The reference landmarks used for imaging and histopathological correlation were the prostatic apex, base and urethra. The mp-MRI images were analysed using axial cuts to facilitate visualization of the tumour lesions marked on whole mount pathology. In this study, tumour size was defined using the cross sectional area, which was calculated as a product of the length radius (measured parallel to a line drawn from right to left of the gland through the middle of the urethra divided by 2, R1), and the width

radius (R2) which was measured from the anterior to posterior of the gland in a line drawn perpendicular to the length, divided by 2. The mathematical formula was based on the area of an ellipse ($\pi \times R1 \times R2$).

2.2. Mp-MRI acquisition

All patients underwent a high field mp-MRI examination, which was obtained with a 3-T MRI imaging system (Magnetom Verio; Siemens, Erlangen, Germany), using a multichannel pelvic phased array coil. The MRI protocols included high spatial resolution T2-weighted imaging in the axial, sagittal and coronal planes (turbo spin echo sequences), diffusion weighted imaging in the axial plane (b-values: 0–50, 500 and 1000 s/mm^2) and dynamic contrast-enhanced (DCE) images. The acquisition parameters were summarized in supplementary Table S1. Apparent diffusion coefficient maps were generated from the diffusion weighted images by using the mono-exponential model on a voxel-wise basis, fitting the b-value data. For the DCE MRI, gadoterate meglumine (DOTAREM®; Guerbet LLC, Villepinte, France), was administered via an automatic power injector (Medrad, PA, Warrendale, USA) at a dose of 0.1 mmol/kg body weight at a rate of 3 mL/s. An endorectal coil was not used. A single dedicated genitourinary radiologist (with 8 years of experience in reading prostate MRI) retrospectively evaluated and scored all lesions. All assessments were made on a commercial PACS workstation (Carestream, Rochester, NY, USA). Each suspicious lesion detected on mp-MRI was assigned a PI-RADS score in accordance with the PI-RADSv2 criteria.

2.3. Histopathological preparation

All prostatectomy specimens were macroscopically examined and weighed. The base and apex were sampled using the conical method [7]. The remaining prostate surfaces (anterior, posterior, right and left) were inked in different colours for orientation and for determining the surgical margins. A positive surgical margin was defined as tumour reaching inked surfaces. The specimens were sequentially sliced from apex to base of the glands at 3–5 mm intervals, and embedded in paraffin as whole-mount sections. The entire specimen was submitted for histological examination by a senior uro-pathologist (with at least 10 years experience in genitourinary pathology). The sections were stained with hematoxylin and eosin. Each tumour focus was marked out on the glass slide and localized onto histological maps, recording its Gleason grade, location and dimensions. Tumours of similar GS, and less than 1 mm apart in the same plane, were considered part of the same lesion. All malignant foci were included in this study regardless of size. The radiologist and pathologist were blinded to their mutual findings prior to data analysis.

2.4. Data analysis

The data analysis was performed using the presumption that each tumour lesion was discrete and independent. The correlation between PI-RADS scores and Gleason grades was calculated using generalized logistic regression. The limits of tumour detection on mp-MRI were determined using binary logistic regression by comparing mp-MRI detection rate against tumour size. We used Fisher's exact test for the correlation between mp-MRI detected lesions and pathological cancer foci, and weighted Kappa coefficient for the association between MRI staging and pathological staging. Statistical significance was defined as $p < 0.05$. The SAS 9.3 software (SAS Institute, Cary, NC, USA) was used to perform statistical analyses.

3. Results

3.1. Patient and tumour characteristics

There were 39 suitable patients with a median age of 64 years. Most of the patients had MRI scans performed post prostate biopsy (90%, $n = 35$). The median time interval between prostate biopsy and mp-MRI was 30 days (range 7–176 days). There were a total of 93 tumour foci identified on whole mount histology, comprising lesions of GS 6 ($n = 28$, 30%), GS 7 ($n = 54$, 58%) and GS ≥ 8 ($n = 11$, 12%). The patient and tumour foci characteristics are summarized in Table 2.

3.2. Evaluation of mp-MRI in detecting prostate cancer

Among the 93 lesions documented on pathology, 63 (68%) were detected and 30 (32%) were missed (false negatives) on mp-MRI. Therefore, the sensitivity and positive

Table 2 Summary of patient demographics and lesion characteristics.

Patient and tumour characteristics	Values
Patient characteristics	
Number of patients	39
Median age, year (range)	64 (45–74)
Post-biopsy MRI, *n* (%)	35 (90%)
Pre-biopsy MRI, *n* (%)	4 (10%)
Median interval from biopsy to MRI, days (range)	30 (7–176)
Lesion characteristics	
MRI suspicious lesions, *n*	81
Malignant on histology, *n* (%)	63 (78%)
Benign on histology, *n* (%)	18 (22%)
PI-RADSv2 score	
3, *n* (%)	18 (22%)
4–5, *n* (%)	63 (78%)
Cancer foci identified on pathology, *n*	93
Mp-MRI detected, *n* (%)	63 (68%)
Mp-MRI missed, *n* (%)	30 (32%)
Gleason score	
6, *n* (%)	28 (30%)
7, *n* (%)	54 (58%)
≥8, *n* (%)	11 (12%)

Analyses were performed on a per lesion basis.
Mp-MRI, multiparametric MRI; MRI, magnetic resonance imaging; PI-RADSv2, Prostate Imaging Reporting and Data System version 2.0.

predictive values of mp-MRI in detecting prostate cancer in this study were 68% (95% CI: 57%—77%) and 78% (95%CI: 67%—86%), respectively.

3.3. Correlation of mp-MRI and pathological findings

Of the 63 lesions detected on mp-MRI, they comprised GS 6 ($n = 13$, 21%), GS 7 ($n = 41$, 65%) and GS ≥ 8 ($n = 9$, 14%). Of the GS 6 lesions, they were classified as PI-RADS 3 in six and PI-RADS 4—5 in seven. Of the GS 7 lesions, the mp-MRI grading were PI-RADS 3 in eight and PI-RADS 4—5 in 33. All lesions with GS ≥ 8 were graded PI-RADS 4—5 on mp-MRI. The mp-MRI detection rates in relation to tumour grades were: 48% (13/27) for GS 6, 75% (41/55) for GS 7, and 82% (9/11) for GS ≥ 8 lesions. Higher Gleason grade cancer lesions were associated with higher PI-RADS scores (odds ratio [OR] = 3.53, 95% CI: 0.93—13.45, standard error [SE] = 0.68, $p = 0.064$, for GS 7 lesions correlating with PI-RADS 4—5). In associating radiological and pathologic stage, the weighted Kappa value was 0.69 ($p < 0.0001$). When analysing all lesions as a cohort, there was no significant relation between tumour detection and its location ($p = 0.62$ by Fisher's exact test).

3.4. Determination of tumour size detection limit on mp-MRI

In estimating the limits of tumour size detection on mp-MRI in this study population, the probability of cancer detection on mp-MRI was compared against tumour size measured on whole mount histology (Fig. 1). For a cancer lesion with a surface area of 20 mm^2 (approximately 5 mm $\times$ 5 mm in diameter), the probability of detection was 50%; for a lesion 100 mm^2 in size (approximately 11 mm $\times$ 11 mm in diameter), its probability of detection was 75%. The overall median tumour size in this study was 57 mm^2 (range 1.6—955.0 mm^2).

3.5. Characteristics of tumour lesions missed on mp-MRI

There were 30 cancer foci identified on whole mount histology that were not detected on mp-MRI, giving a false negative rate of 32%. These comprised GS 6 (n = 15), GS 7 ($n = 13$) and GS ≥ 8 ($n = 2$) lesions. The median size of these missed lesions was 19 mm^2 (range 2—220 mm^2). The locations of these missed lesions were apex ($n = 16$, 54%), mid-gland ($n = 7$, 23%) and base ($n = 7$, 23%). In a subgroup analysis of cancer foci larger than 10 mm in diameter (in any dimension), there were 51 such lesions, of which eight (16%) were missed on mp-MRI. Of these missed large lesions, 88% (7/8) involved the apical location. On histology, 50% (4/8) had narrow footprints on cross section (Table 3).

3.6. The impact of time interval between prostate needle biopsy and acquisition of mp-MRI images

Within the 35 patients who had mp-MRI performed after prostate biopsy, a total of 83 cancer foci were identified on

Table 3 Characteristics of missed large lesions.

Patient No.	GS	Length (mm)	Width (mm)	Area (mm^2)	Location
1	7	14	2	22	AM
2	7	11	3	25	AM
3	7	18	4	55	AM
4	6	36	2	57	A
5	8	12	9	85	AM
6	7	18	10	137	A
7	7	14	15	165	MB
8	7	28	10	220	AM

All measurements taken were based on cross sectional whole-mount sections of the prostate glands at 3—5 mm intervals. Large lesions were those that were at least 10 mm in any one dimension. A, apex; AM, apex to mid-gland; GS, Gleason score; MB, mid-gland to base.

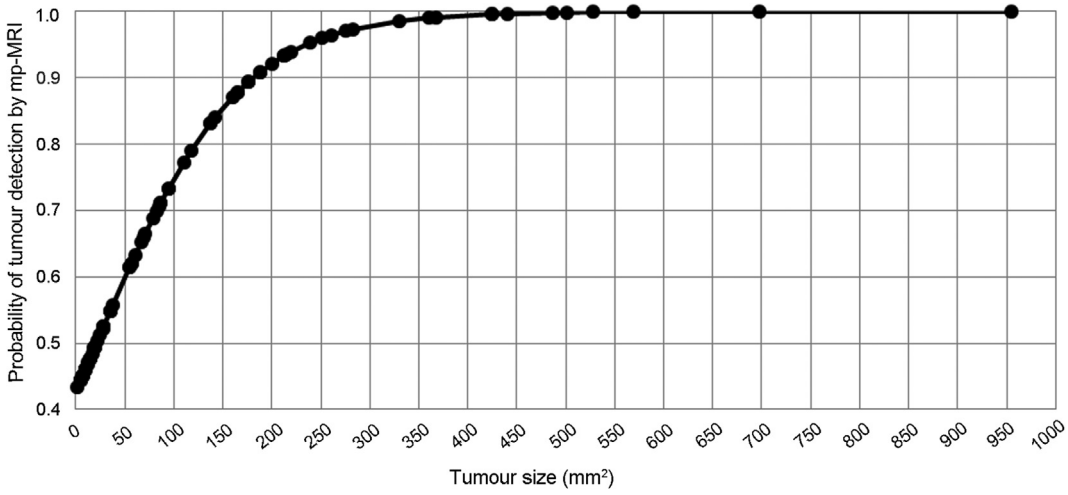

Figure 1 Size detection limits of cancer by multi-parametric magnetic imaging resonance (mp-MRI). Probability of tumour detection was calculated using binary logistics regression. Tumour size was defined as the largest cross sectional areas of cancer foci on pathology in square millimeters.

pathology. These were dichotomized into two groups: Less than 6 weeks ($n = 26$) and greater than or equal to 6 weeks ($n = 57$). The false negative rates were 31% (8/26) for less than 6 weeks, and 33% (19/57) for greater or equal to 6 weeks.

4. Discussion

This study represents the first few in literature correlating the performance of PI-RADSv2 in detecting prostate cancer using radical prostatectomy specimens as a standard of reference. Previous studies using needle biopsy tissue diagnosis and localization may have outcomes influenced by technical constraints of the biopsy process, including anatomical locality and the sensitivity of tumour detection [8–13]. These limitations were overcome, in this study, by using radical prostatectomy specimens as reference standard for anatomical and pathological correlation. Of note, anatomical distortion during mp-MRI image acquisition was minimized as there was no utilization of an endorectal coil. There was also awareness that post-processing changes occurring during specimen preservation may confound the correlation between imaging and histopathology. These potential confounders were largely overcome by adopting fixed anatomical points of reference comprising the urethra, prostatic base and apex, which were unlikely to be modified after paraffin embedding.

It was well recognized that post-biopsy artefacts may confound the imaging analysis, and hence there has been a preference towards acquisition of pre-biopsy mp-MRI images [14,15]. However, it is still the predominant practice to perform mp-MRI after histological diagnosis of cancer. Within this clinical context, the outcomes from this study could guide clinicians in disease localization and planning of treatment. This is especially relevant in pre-operative surgical planning for laterality of nerve-sparing. The risk of missing a significant apical lesion in this series was 35%. It was recognized that positive surgical margins were largely apical in location and, therefore, where a pre-biopsy MRI was not possible, adequate apical sampling during needle biopsy would be warranted [16,17]. The lesions missed on mp-MRI also tend to have a narrow footprint on cross sectional imaging, which can make radiological detection challenging in the transverse cross section.

The existing recommendations propose a minimum time interval of 6 weeks between performing the needle biopsy and mp-MRI [18]. However, an exploratory analysis in this study comparing the proportion of lesions missed on mp-MRI, which performed within or after a 6 week time intervals from biopsy, showed no difference in the false negative rates of tumour detection (30%). In addition, hemorrhagic artefacts could be seen at the scans performed 6 weeks after biopsy, degrading the interpretation of the mp-MRI data (Fig. 2). These suggested that the optimal time interval for mp-MRI after prostate biopsy should be longer than 6 weeks; this will require elucidation in a larger patient cohort comparing pre- and post-biopsy images. There may also be a suggestion that the presence of hemorrhage in post-biopsy scans may not compromise the detection of extra-prostatic disease in the early post-biopsy time period, but only if the reporting radiologists were aware of tumour location(s) at biopsy [19]. In this study, there was no attempt to quantify the extent of post-biopsy hemorrhage, as there is no objective methodology for doing so. The subjective assessment of hemorrhage can also vary between image readers and, thus, is of limited value.

The sensitivity and positive predictive values (PPV) for our study were 0.68 and 0.78 respectively, which were similar to the diagnostic performance of the original PI-RADS, based on a meta-analysis of 14 studies by Hamoen et al. [4]. In that review, the pooled sensitivity was 0.78 with PPV ranging from 0.50 to 0.83. However, most of the histological correlation was made with prostate biopsy outcomes, rather than a gold standard of prostatectomy histopathology. More recently, some authors have reported an improved diagnostic accuracy when mp-MRI included magnetic resonance spectroscopy imaging (MRSI) [20,21]. The authors reported a high negative predictive value of 0.93 in a cohort with prostate specific antigen (PSA) values of <10 ng/mL, suggesting a utility of mp-MRI in identifying patients who will have negative biopsies [22]. When comparing studies with similar methodology in a meta-analysis by Kirkham et al. [23], the diagnostic efficacy was similar when using both T2 and DCE images (sensitivity

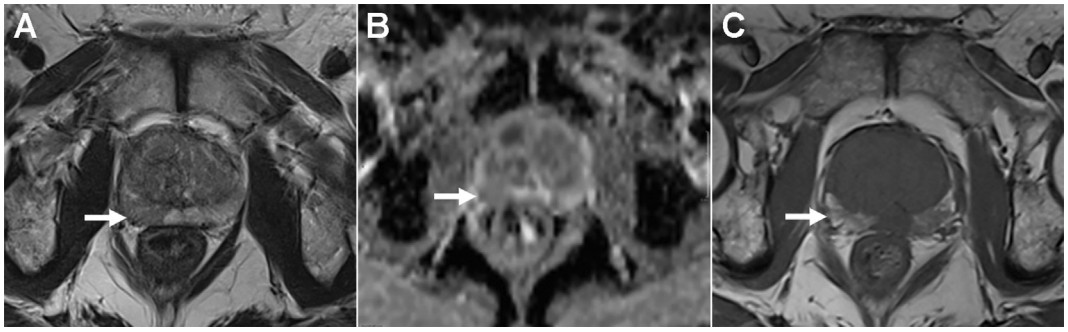

Figure 2 Persistent haemorrhagic changes on magnetic resonance imaging obtained 51 days post transrectal ultrasound needle biopsy. (A) Axial T2-weighted image of prostate at the level of the mid-gland demonstrating an ill-defined, mildly hypointense lesion in the right posterior peripheral zone (arrow). (B) Axial apparent diffusion coefficient map of the prostate at the same level demonstrating the lesion as a mildly hypointense signal (arrow). The lesion was isointense on diffusion weighted images (not shown). (C) Axial T1-weighted image demonstrates hemorrhage appearing as a hyperintense signal (arrow), limiting the assessment of dynamic contrast enhanced images. Histology showed a corresponding Gleason score 6 ($3 + 3$) lesion.

0.73—0.89) referenced to histological outcomes at prostatectomy, with inclusion of all tumour lesions. However, it was not clear if these studies looked at pre- or post-biopsy cohorts.

In a study comparing PI-RADSv2 with version 1, using MRI-guided biopsy results as the reference standard, Polanec et al. [24] reported a higher sensitivity for lesions in the transitional zone (TZ), but lower in the peripheral zone (PZ); the overall sensitivity using PI-RADSv2 was close to 100%. In another retrospective study by Vargas et al. [25], the authors correctly classified 95% of tumours of any grade $\geq$0.5 mL in size with PI-RADSv2, which decreased to 20%—26% for GS $\geq$ 7 tumours that were $\leq$0.5 mL. This study was not designed to be a diagnostic accuracy study, and pathologically detected tumours were used as a template to classify MRI detected lesions.

The characteristics of missed lesions in this study were those of small physical dimensions (median size being 19 mm^2, which is approximately 5 mm in diameter), and lower GS. This was also similarly shown in earlier studies using different radiological reporting systems [26,27]. In those studies, lesions located in the apex were more likely to be missed. The inclusion of all visible lesions on histopathology allowed for determination of the size detection limit for mp-MRI in the post-biopsy setting. This was in contrast to other studies where small lesions ($<$0.5 mL volume) of lower grade were excluded [27]. In the subgroup analysis of large lesions that were missed on mp-MRI (defined as at least 10 mm in any one dimension), the majority were located in the apex. Furthermore, half of these had narrow footprints on cross section (Fig. 3). This finding suggested that a good sampling of the apex during needle biopsy of the prostate gland is important, and should be strongly recommended. Careful attention must therefore be paid when dissecting the apex during radical prostatectomy.

There are limitations in this study. The inherent shortcomings of a limited size cohort include the phenotypic expression of cancer lesions, where a group of tumour foci from the same prostate specimen may share MRI characteristics that could affect analysis on a per lesion basis. The population studied was limited by the selection criteria of surgical candidates. The majority of lesions were of pathological GS 7, which reflect a contemporary practice of offering active surveillance for GS 6 tumours [16]. Patients operated in our institution, but with mp-MRI scans performed not within our protocol, were excluded. However, it is not evident that these patients are inherently different in characteristics from the study population. The radiologist analysing the mp-MRI images was not blinded to the diagnosis of malignancy, although there was no prior knowledge of the exact anatomical location of each tumour foci on whole mount histology. Mp-MRI interpretation by a single radiologist reader directly impacts on the outcome of this study. It is difficult to quantify the effect of the learning curve using PI-RADSv2 on sensitivity and specificity. However, the significant background clinical experience of the reader is expected to shorten the learning process.

In this predominantly post-biopsy cohort of organ confined prostate cancer patients, mp-MRI using PI-RADSv2 showed good correlation with the histological and

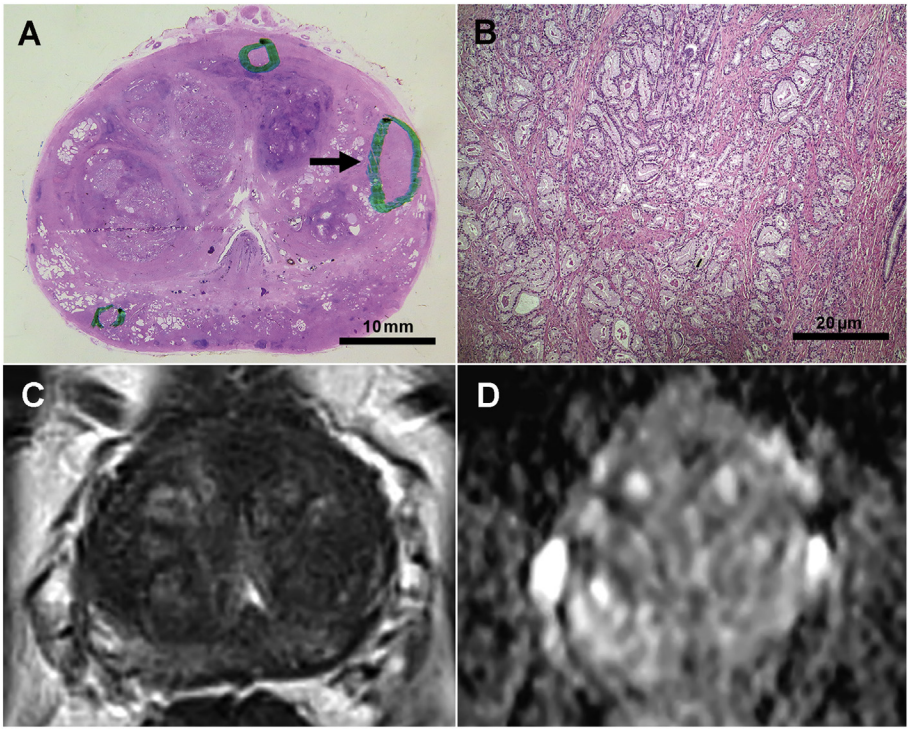

Figure 3 Disc-shaped tumour lesion missed on multiparametric-magnetic resonance imaging. (A) Wholemount histopathology section at the level of mid-gland, showing a tumour focus at the peripheral zone in the left lateral position measuring 18 mm $\times$ 4 mm (black arrow); (B) Histology revealed Gleason score 7 (3 + 4) cancer (Haemotoxylin and Eosin [H&E] stain, $\times$ 40 magnification); (C) and (D) Axial T2-weighted and diffusion-weighted images of the same prostate gland at the same level did not demonstrate the lesion seen on histology.

anatomical profile of tumours detected on whole mount prostatectomy histopathology, providing predictive information on tumour grade, location and size. The post-biopsy changes may post a challenge to the mp-MRI detection of smaller tumours, especially those apical in locations and with narrow footprints on cross sections. Nevertheless, this study still provides a useful guide for planning treatment strategy in a practice where mp-MRI scans are commonly done after tissue diagnosis of prostate cancer is made. These results may not be generalizable to practices where a dedicated radiological service observing stringent protocols for image acquisition and a dedicated reader to interpret mp-MRI images are not available.

5. Conclusion

Mp-MRI scans of the prostate gland using PIRADSv2 reporting provides predictive information on tumour grade, location and size, and even in a post-biopsy setting. The findings of this study can help guide urologists in the planning of local treatment strategy to optimize patient outcomes.

Author contributions

Study concept and design: Edwin Jonathan Aslim, Yan Mee Law, Lui Shiong Lee.
Data acquisition: Edwin Jonathan Aslim, Yan Mee Law, Viswanath Anand Chidambaram.
Drafting of manuscript: Edwin Jonathan Aslim, Yan Mee Law, Viswanath Anand Chidambaram, Lui Shiong Lee.
Critical revision of the manuscript: Puay HoonTan, John Carson Allen Jr, Lionel Tim-Ee Cheng, Li Yan Khore, Benjamin Yongcheng Tan, Christopher Wai Sam Cheng, John Shyi Peng Yuen, Henry Sun Sien Ho, Lui Shiong Lee.
Final approval of manuscript: Yan Mee Law, Puay Hoon Tan, Lui Shiong Lee.

Conflicts of interest

The authors declare no conflict of interest.

Appendix A. Supplementary data

Supplementary data related to this article can be found at https://doi.org/10.1016/j.ajur.2018.05.008.

References

[1] Kitajima K, Kaji Y, Fukabori Y, Yoshida Ki, Suganuma N, Sugimura K. Prostate cancer detection with 3 T MRI: comparison of diffusion-weighted imaging and dynamic contrast-enhanced MRI in combination with T2-weighted imaging. J Magn Reson Imag 2010;31:625—31.
[2] Dickinson L, Ahmed HU, Allen C, Barentsz JO, Carey B, Futterer JJ, et al. Scoring systems used for the interpretation and reporting of multiparametric MRI for prostate cancer detection, localization, and characterization: could standardization lead to improved utilization of imaging within the diagnostic pathway? J Magn Reson Imag 2013:3748—58.
[3] Barentsz JO, Richenberg J, Clements R, Choyke P, Verma S, Villeirs G, et al. ESUR prostate MR guidelines 2012. Eur Radiol 2012;22:746—57.
[4] Hamoen EH, de Rooij M, Witjes JA, Barentsz JO, Rovers MM. Use of the prostate imaging reporting and data system (PI-RADS) for prostate cancer detection with multiparametric magnetic resonance imaging: a diagnostic meta-analysis. Eur Urol 2015;67:1112—21.
[5] Barrett T, Turkbey B, Choyke PL. PI-RADS version 2: what you need to know. Clin Radiol 2015;70:1165—76.
[6] Auer T, Edlinger M, Bektic J, Nagele U, Herrmann T, Schäfer G, et al. Performance of PI-RADS version 1 versus version 2 regarding the relation with histopathological results. World J Urol 2016:1—7.
[7] Tan PH, Cheng L, Srigley JR, Griffiths D, Humphrey PA, Van Der Kwast TH, et al. International Society of Urological Pathology (ISUP) consensus conference on handling and staging of radical prostatectomy specimens. Working group 5: surgical margins. Mod Pathol 2011;24:48—57.
[8] Roethke MC, Kuru TH, Schultze S, Tichy D, Kopp-Schneider A, Fenchel M, et al. Evaluation of the ESUR PI-RADS scoring system for multiparametric MRI of the prostate with targeted MR/TRUS fusion-guided biopsy at 3.0 Tesla. Eur Radiol 2014; 24:344—52.
[9] Thompson JE, Moses D, Shnier R, Brenner P, Delprado W, Ponsky L, et al. Multiparametric magnetic resonance imaging guided diagnostic biopsy detects significant prostate cancer and could reduce unnecessary biopsies and over detection: a prospective study. J Urol 2014;192:67—74.
[10] Schimmöller L, Quentin M, Arsov C, Hiester A, Buchbender C, Rabenalt R, et al. MR-sequences for prostate cancer diagnostics: validation based on the PI-RADS scoring system and targeted MR-guided in-bore biopsy. Eur Radiol 2014;24: 2582—9.
[11] Cash H, Maxeiner A, Stephan C, Fischer T, Durmus T, Holzmann J, et al. The detection of significant prostate cancer is correlated with the Prostate Imaging Reporting and Data System (PI-RADS) in MRI/transrectal ultrasound fusion biopsy. World J Urol 2016;34:525—32.
[12] Fascelli M, Rais-Bahrami S, Sankineni S, Brown AM, George AK, Ho R, et al. Combined biparametric prostate MRI and prostate specific antigen in the detection of prostate cancer: a validation study in a biopsy naive patient population. Urology 2016;88:e34.
[13] Grey ADR, Chana MS, Popert R, Wolfe K, Liyanage SH, Acher PL. Diagnostic accuracy of magnetic resonance imaging (MRI) prostate imaging reporting and data system (PI-RADS) scoring in a transperineal prostate biopsy setting. BJU Int 2015;115:728—35.
[14] Radtke JP, Kuru TH, Boxler S, Alt CD, Popeneciu IV, Huettenbrink C, et al. Comparative analysis of transperineal template saturation prostate biopsy versus magnetic resonance imaging targeted biopsy with magnetic resonance imaging-ultrasound fusion guidance. J Urol 2015; 193:87—94.
[15] Lee DJ, Recabal P, Sjoberg DD, Thong A, Lee JK, Eastham JA, et al. Comparative effectiveness of targeted prostate biopsy using MRI-US fusion software and visual targeting: a prospective study. J Urol 2016;196:697—702.
[16] Alvin LW, Gee SH, Hong HH, Christopher CW, Henry HS, Weber LK, et al. Oncological outcomes following robotic-assisted radical prostatectomy in a multiracial Asian population. J Robot Surg 2015;9:201—9.
[17] Dev HS, Wiklund P, Patel V, Parashar D, Palmer K, Nyberg T, et al. Surgical margin length and location affect recurrence rates after robotic prostatectomy. Urol Oncol 2015;33. 109.e7—13.

[18] Weinreb JC, Barentsz JO, Choyke PL, Cornud F, Haider MA, Macura KJ, et al. PI-RADS prostate imaging—reporting and data system: 2015, version 2. Eur Urol 2016;69:16—40.
[19] Sharif-Afshar AR, Feng T, Koopman S, Nguyen C, Li Q, Shkolyar E, et al. Impact of post prostate biopsy hemorrhage on multiparametric magnetic resonance imaging. Can J Urol 2015;22:7698—702.
[20] Perdonà S, Di Lorenzo G, Autorino R, Buonerba C, De Sio M, Setola SV, et al. Combined magnetic resonance spectroscopy and dynamic contrast-enhanced imaging for prostate cancer detection. Urol Oncol 2013;31:761—5.
[21] Fusco R, Sansone M, Petrillo M, Setola SV, Granata V, Botti G, et al. Multiparametric MRI for prostate cancer detection: preliminary results on quantitative analysis of dynamic contrast enhanced imaging, diffusion-weighted imaging and spectroscopy imaging. Magn Reson Imag 2016; 34:839—45.
[22] Petrillo A, Fusco R, Setola SV, Ronza FM, Granata V, Petrillo M, et al. Multiparametric MRI for prostate cancer detection: performance in patients with prostate-specific antigen values between 2.5 and 10 ng/mL. J Magn Reson Imag 2014;39:1206—12.
[23] Kirkham AP, Emberton M, Allen C. How good is MRI at detecting and characterising cancer within the prostate? Eur Urol 2006;50:1163—75.
[24] Polanec S, Helbich TH, Bickel H, Pinker-Domenig K, Georg D, Shariat SF, et al. Head-to-head comparison of PI-RADS v2 and PI-RADS v1. Eur J Radiol 2016;85:1125—31.
[25] Vargas HA, Hotker AM, Goldman DA, Moskowitz CS, Gondo T, Ehdaie B, et al. Updated prostate imaging reporting and data system (PIRADS v2) recommendations for the detection of clinically significant prostate cancer using multiparametric MRI: critical evaluation using whole-mount pathology as standard of reference. Eur Radiol 2016;26:1606—12.
[26] De Visschere PJL, Naesens L, Libbrecht L, Van Praet C, Lumen N, Fonteyne V, et al. What kind of prostate cancers do we miss on multiparametric magnetic resonance imaging? Eur Radiol 2016;26:1098—107.
[27] Tan N, Margolis DJ, Lu DY, King KG, Huang J, Reiter RE, et al. Characteristics of detected and missed prostate cancer foci on 3-T multiparametric MRI using an endorectal coil correlated with whole-mount thin-section histopathology. AJR Am J Roentgenol 2015;205:W87—92.